Drag reduction design and experiments for the chisel-shaped shovel tip

Longlong Wang, Changjiang Zheng, Mingke Li, Tongtong Mi, Songze Li, Xuemei Yi

Publisher's Disclaimer

E-publishing ahead of print is increasingly important for the rapid dissemination of science. The *Early Access* service lets users access peer-reviewed articles well before print/regular issue publication, significantly reducing the time it takes for critical findings to reach the research community.

These articles are searchable and citable by their DOI (Digital Object Identifier).

Our Journal is, therefore, e-publishing PDF files of an early version of manuscripts that undergone a regular peer review and have been accepted for publication, but have not been through the typesetting, pagination and proofreading processes, which may lead to differences between this version and the final one.

The final version of the manuscript will then appear on a regular issue of the journal.

Please cite this article as doi: 10.4081/jae.2024.1576

Drag reduction design and experiments for the chisel-shaped shovel tip

Longlong Wang, Changjiang Zheng, Mingke Li, Tongtong Mi, Songze Li, Xuemei Yi

College of Mechanical and Electronic Engineering, Northwest A&F University, Yangling, Shaanxi, China

Correspondence: Xuemei Yi, College of Mechanical and Electronic Engineering, Northwest A&F University, Yangling 712100, Shaanxi, China.
Tel.: +86.15388627635.
E-mail: xuemei_yi@nwsuaf.edu.cn

Key words: chisel-shaped shovel tip; shark skin; V-shaped structure; discrete element method simulation; drag reduction.

Abstract

To address the issue of high resistance encountered by traditional chisel-shaped shovel tips during tillage, this study drew inspiration from the micro V-shaped structures found in shark skin. Using laser cladding technology, a V-shaped wear-resistant coating was applied to the front surface of the shovel, with different drag-reducing V-shaped structures achieved by controlling the coating overlap ratio H (including 20%, 40%, and 60%). Additionally, the rear surface of the shovel tip was designed to mimic the V-shaped morphology of shark skin, proportionally amplified, and given a certain backward tilt angle θ to further reduce resistance. Through the discrete element simulation experiments while maintaining θ at 0°, it was found that the shovel tip achieved the best drag reduction effect when H was 40%. Based on this, the study varied the values of θ (including 0°, 1°, 3°, and 5°) while keeping H at 40%. Discrete element simulation experiments were conducted at depths of 250mm, 275mm, and 300mm to analyze the disturbance effect, fragmentation effect, and resistance of the shovel tip. Considering all factors, the shovel tip with θ of 5° was selected as the optimal choice. Finally, a soil trench experiment was conducted to verify the performance of the V-shaped shovel tip with H of 40% and θ of 5°, as well as the chisel-shaped shovel tip, in tillage operations. The experimental results showed good agreement with the simulation results, and the designed V-shaped shovel tip achieved a maximum drag reduction of 12.87%. This design provides valuable references for the structural optimization of subsoiler, contributing to the improvement of their performance and efficiency.

Introduction

Tillage is an important core technique in conservation tillage, which aims to break up the plow bottom layers, improve its water permeability and air ventilation, and ultimately increase crop yield(Zheng et al., 2019; Torres et al., 2022). However, the commonly used chisel-shaped subsoiler encounters resistance from various rocks and plant roots during tillage operation, resulting in increased traction energy consumption, accelerated wear of the shovel, reduced efficiency and quality of tillage operations, and significant economic losses(Martins et al., 2023). Currently, drag reduction methods for tillage mainly include electronic permeation drag reduction, vibration-based drag reduction, and structural optimization drag reduction. However, electronic permeation and vibration-based methods still face challenges such as high energy consumption and complex

structures(Niu et al., 2022). Therefore, it is necessary to optimize the structure of the traditional chisel-type subsoiler in order to reduce the resistance encountered during tillage operations.

In recent years, biomimetics has been increasingly applied to the structural optimization of agricultural machinery to achieve drag reduction(Song et al., 2022; Zhang et al., 2022). Wu et al. applied the surface structural characteristics of ant's tarsi to the design of a shovel tip, achieving a reduction in tillage resistance by 24.6% to 33.7%(Wu et al., 2021). Jia et al. applied the drag-reducing characteristics of rabbit's claw toes to the design of a subsoiler, resulting in a reduction in tillage resistance by 13% to 19%(Jia et al., 2019). Bai et al. applied the curve of a badger's claw to the design of a subsoiler, resulting in a reduction in resistance by 13.05% to 18.94%(Bai et al., 2016). Zhang et al. applied the head curve of a sandfish lizard to the design of a subsoiler, achieving a reduction in tillage resistance by 8.43% to 19.31% in simulation experiments (Zhang et al., 2021).The shark skin surface features a V-shaped structure parallel to the direction of shark movement, effectively reducing resistance during swimming(Ma et al., 2016; Wu et al., 2018;). Pu et al. confirmed the outstanding drag reduction performance of shark skin microstructure through their study of this structure and its mechanical behavior(Pu et al., 2016). ZHANG et al. conducted drag reduction experiments by applying the V-shaped structure in a vacuole water tunnel, resulting in a reduction of resistance by 8% to 12%(ZHANG et al., 2011). Li et al. applied the V-shaped structure to the surface of fish-like robots, observing a 6.6% increase in robot speed and a 5.9% reduction in energy consumption(Li et al., 2014). Sun et al. successfully reduced energy consumption by applying the V-shaped structure of shark skin to a deep-tillage shovel, validating its drag reduction effect through simulation analysis and experiments(Sun et al., 2018).

In order to fully achieve drag reduction in the design, this study is based on the principles of biomimetics and combines the micro V-shaped structures found in shark skin to design the front and rear surfaces of the chisel-type shovel tip. Through simulations, the disturbance effect, fragmentation effect, and tillage resistance of the chisel-shaped shovel tip and the V-shaped shovel tip are obtained. A comprehensive analysis is conducted to determine the optimal shovel tip design. A comparison is made between the simulation and experimental results to validate the effectiveness of the discrete element method, providing a theoretical foundation and design basis for energy-saving and drag reduction in deep loosening operations.

Material and Methods

Analysis of drag resistance in subsoiler

The shovel tip and handle of the subsoiler used in this study are made of 65Mn steel and comply with the specifications of the Chinese standard JB/T 9788-1999. The subsoiler consists of the shovel tip segment, plow bottom arc segment, cultivation layer arc segment, and straight handle segment, as shown in Figure 1a. At different depths, the tillage resistance and wear distribution in different functional zones of the subsoiler follow the pattern of shovel tip segment > plow bottom arc segment > cultivation layer arc segment > straight handle segment. At the same time, severe wear at the front end of the shovel tip during the tillage process leads to shovel tip fracture(Wang et al., 2021), as shown in Figure 1b. Therefore, to achieve maximum drag reduction and minimize wear, this study focuses on the design of the chisel-shaped shovel tip.

Shovel tip design

Sharks are widely used in drag reduction designs due to their ability to move rapidly in water(Hu et al., 2007; Wang et al., 2020). In this study, the scalloped hammerhead shark, known for its fast swimming speed, was selected as the research subject. By observing the skin structure of the shark, it was found that its shape resembles a V-shape(Zhao et al., 2012; Kim et al., 2014), as shown in Figure 1c. This V-shaped structure effectively controls the turbulent flow on the surface of the shark's body, serving as a means of flow redirection and thus reducing the drag experienced by the shark during swimming(Dean et al., 2010; Yan et al., 2023).Therefore, in this study, the V-shaped structure is applied to the design of the chisel-shaped shovel tip, aiming to reduce the resistance during the operation of the subsoiler and utilize the flow redirection effect of the V-shaped grooves to improve the efficiency of soil tillage.

Drag reduction design at the front end of the shovel tip surface

Laser cladding is a novel surface modification technique that typically produces coatings with high hardness and wear resistance, exhibiting a V-shaped morphology as shown in Figure 1d(Agrawal et al., 2020; Xu et al., 2021; Shan et al., 2022). The tungsten carbide (WC) particles have a high melting point, high hardness, and excellent wear resistance. Compared to other traditional ceramic

materials, they exhibit better thermal stability and wetting properties. As a result, they are widely used in laser cladding for coating metal-based ceramic materials, aiming to enhance the wear resistance of critical components(Li et al.,2023). Therefore, in this study, laser cladding technology was employed to address the issues of wear and fatigue fracture at the front end of the shovel tip surface of the subsoiler and achieve drag reduction. The commonly used parameters for laser cladding were WC content of 25 wt%, powder thickness of 1.0 mm, laser scanning speed of 10 mm/s, and laser power of 1000 W(Chen et al., 2015). Additionally, the overlap rate H was used as a variable to control the V-shaped structure. In practical production, the overlap rate H is typically controlled between 20% and 60% to ensure the quality of cladding. Thus, this paper intends to investigate the influence of three gradient values of H (20%, 40%, and 60%) on the drag reduction performance.

Drag reduction design at the rear end of the shovel tip surface

Due to the fixed size of the shovel tip, when there are too many V-shaped structures, the surface tends to become flat, which cannot simulate the grooves between each V-shaped structure. On the other hand, when there is only one V-shaped structure, it fails to achieve the desired flow diversion effect due to the absence of grooves. Therefore, in this study, the V-shaped structure of shark skin was fitted and two V-shaped structures were proportionally enlarged. Additionally, a backward inclination angle θ was applied to the rear end of the shovel tip surface coated with laser cladding, as shown in Figure 1d(Wang *et al*., 2022).

The shear and compression ability of V-shaped structures is influenced by the longitudinal angle between the V-shaped structures and the soil. As the longitudinal angle decrease, a greater amount of soil is simultaneously sheared. However, the drag reduction effect provided by drainage gradually diminishes in the V-shaped grooves. At the same time, the arc-shaped handle used for both the V-shaped shovel tip and the chisel-shaped shovel tip is the same, resulting in an entry angle of 23°. This angle exceeds the friction angle between the soil and the material of the shovel tip (65Mn steel). Excessively increasing the θ value would make it difficult for the soil to move in the opposite direction along the V-shaped groove towards tillage. Therefore, to determine the optimal θ value, this study conducted experiments with smaller θ values of 0°, 1°, 3°, and 5°. By conducting a comprehensive analysis of soil disturbance, soil fragmentation effect, and average resistance of the

shovel tip at different θ values, the optimal θ can be determined. Therefore, to find the optimal θ, this study conducted experiments with θ values of 0°, 1°, 3°, and 5°. By comprehensively analyzing the soil disturbance , soil fragmentation effect, average resistance, and other indicators of the shovel tip under different θ values, the optimal θ can be determined.

Working principle

The shovel tip and handle shear and compress the soil under the action of traction force. This shearing action creates large and small soil particles. The small soil particles are directed by the flow effect of the V-shaped grooves to move in the opposite direction of tillage, as shown in Figure 2a. On the other hand, the large soil particles tend to accumulate at the shovel tip due to the lesser flow effect of the grooves and are subsequently lifted upward and undergo failure fragmentation under the action of the shovel, as shown in Figure 2b. The lifting of soil disturbs the cultivation layer, resulting in the formation of soil ridges on the ground surface, as shown in Figure 2c. Subsequently, the soil ridges on the ground surface undergo failure fragmentation under the shearing action of the straight section of the handle, and finally, under the influence of gravity, they move downward and backward along the cutting edge of the straight section of the handle and backfill the loosened groove.

Establishment of simulation model

Subsoiler model

This study utilizes SOLIDWORKS software to create a 3D model of the deep-tillage shovel specified in the Chinese standard JB/T 9788-1999, maintaining a 1:1 scale, and saves it in ".igs" format, as shown in Figure 3a. During the simulation, the shovel tip model undergoes multiple replacements. Here, only one variant of the V-shaped shovel tip is presented.

Soil model

The soil samples used in this study were collected from the experimental field at the North Campus of Northwest A&F University, located in Yangling Demonstration Zone, Shaanxi Province, China. This experimental field undergoes regular tillage and provides real agricultural soil data. According to the Chinese Soil Classification Standard (GB/T 17296-2009) and measurement

methods described in relevant literature (Li et al., 2023), the physical properties of soil samples from the cultivation layer, plow bottom layer, and topsoil layer were tested. The soil particle sizes are as shown in Table 1, and other physical properties are presented in Table 2

In discrete element simulations, as the particle size decreases, the simulation runtime exhibits a geometric progression growth(Zheng *et al*., 2016). Therefore, many researchers choose to use spherical particles with a diameter of 8 millimeters or larger as soil particle models to more accurately simulate the interaction processes between tillage components and soil(Ding *et al*., 2017). To fully simulate the deep loosening process, this study selected particles with diameters of 8 millimeters, 5 millimeters, and 3 millimeters to represent all particles in the soil. The soil model was set up based on the proportions of each particle diameter as shown in Table 1, as detailed in Table 2.

To fully simulate the tillage operation, a soil model with dimensions of 1000×600×400 was created in EDEM software, consisting of a total of 156,000 particles, as shown in Figure 3b. Based on the differences in physical properties of soil particles, the soil model used in the simulation was divided into three layers: the cultivation layer, plow bottom layer, and topsoil layer. The cultivation layer (0-220 mm) is represented by green color, the plow bottom layer (220-300 mm) is represented by blue color, and the topsoil layer (300-400 mm) is represented by red color. Furthermore, the Hertz-Mindlin with bonding contact model was utilized to describe the mechanical interactions between soil particles, and cylindrical bonding elements were used to represent the cohesive bonds between soil particles, which can withstand certain forces and moments(Wang *et al*., 2020), as shown in Figure 3c.

Simulation parameter settings

The simulation process lasted for a total of 13.5 seconds, with the particle generation occurring from 0 to 8 seconds. The complete insertion of the subsoiler into the soil occurred between 10.45 seconds and 11.65 seconds, with a tillage speed of 0.83 m/s. The time step used in the simulation was $3×10^{-5}$ seconds, and data points were saved every 0.05 seconds. The parameters for the discrete element model simulation are presented in Table 1.

Soil trough experiment verification

To validate the rationality of the designed shovel tip, experiments were conducted in the soil trough laboratory at Northwest A&F University. The experiment utilized a four-wheel-drive soil trough experimental power vehicle (TCC-2.1) for traction power. In order to ensure consistency between the experimental soil and the actual field soil, the following steps were taken during the preparation phase: Firstly, a water pipe was fixed below the subsoiler for traction, allowing adjustment of the soil moisture content inside the soil trough. Subsequently, the soil was compacted. After a period of time, the soil compaction and moisture content were measured. Once the parameters matched those of the experimental field soil, the experiment began. The specific process is shown in Figures 4a, 4b, and 4c.

In the soil trough experiment, the test area was divided into a 2m acceleration zone, a 20m effective zone, and a 2m deceleration zone, as shown in Figure 4d. The tillage depths used in the experiment were consistent with the simulated simulations, namely 250mm, 275mm, and 300mm. Under the condition of a speed of 0.83m/s, both the chisel-shaped shovel tip and the V-shaped shovel tip (as shown in Figure 4e) were used, with each shovel type performing 15 tillage operations in the soil trough. Each test consisted of three stages: harrowing, compaction, and tillage, as shown in Figures 4f, 4g, and 4h, respectively.

Bonds' breakage count and soil fragmentation rate reflect the degree of soil fragmentation during the tillage process of the subsoiler. Since it is not feasible to measure Bonds' breakage count in reality, this study validates the simulation results using the soil fragmentation rate. After the completion of the tillage operation, 10 measurement points were taken at intervals of 3 meters along the direction of tillage in the middle of the soil trough. For any selected measurement point, within a 0.5m x 0.5m area, the ratio of the mass of soil clods with a particle size smaller than 40mm to the total mass of soil within the tillage depth range was calculated as the soil fragmentation rate(Hao *et al*.,2023).

Results and Discussion

The impact of H on the tillage resistance

The depth of the plow bottom layer is typically around 220-300mm, and the purpose of tillage is to break up this layer. However, different crops have different planting depths, and it was observed that the subsoiler experiences the highest resistance at a depth of 300mm(Jiang *et al*.,

2020). Therefore, to explore the optimal H for drag reduction, simulations were conducted at a depth of 300mm in this section.

According to Figure 5, it can be observed that the resistance of the subsoiler in the soil decreases initially and then increases with the increase in H. This is because as H increases, the number of V-shaped morphologies increases, resulting in a lower force required for the subsoiler to shear through the soil, and consequently reducing the particle size of the sheared soil. The formation of smaller particle soil increases with the increasing number of V-shaped morphologies and moves in the opposite direction of tillage along the grooves. As a result, the resistance gradually decreases. However, when H continues to increase, the width of the grooves between V-shaped morphologies becomes too small, approaching a flat surface, which leads to the loss of soil drainage function in the grooves. This causes soil accumulation at the upper end of the shovel tip, thereby increasing the resistance.

Based on the consideration of drag reduction effectiveness, this study selects 40% as the optimal H for drag reduction.

The analysis of optimal parameters

In this study, the θ of the shovel tip was varied at increments of 0°, 1°, 3°, and 5° based on a constant H value of 40%. Simultaneously, simulations were conducted at different depths, including 250mm, 275mm, and 300mm, to observe the extent of drag reduction achieved and analyze its impact on the soil(Wang *et al*., 2021). By considering these factors comprehensively, the optimal drag reduction θ was determined.

Disturbance effects on soil

Existing studies have shown that increasing disturbance in deeper soil layers and reducing disturbance in the surface soil can regulate soil water storage and moisture retention. Additionally, to ensure better crop growth, it is advisable to minimize mixing between the plow bottom layer and the cultivation layer (Wang *et al*., 2019; Vanderhasselt *et al*., 2023).

This study utilizes the post-processing capabilities of EDEM to export the rising height of the cultivation layer and the quantity of soil particles in the cultivation layer within the plow bottom layer, as shown in Figure 6.

According to Figure 6, under the same depth and a constant θ, the disturbance range of the cultivation layer is the largest, followed by the plow bottom layer, while the disturbance range of the top soil layer is the smallest. The main reason for this is that during the tillage operation, the shovel tip primarily acts on the plow bottom layer, causing the large particles in the plow bottom layer to move towards the cultivation layer. As a result, the disturbance range in the top soil layer is smaller, while the cultivation layer experiences greater disturbance. This is because the cultivation layer is subject to the upward force exerted by the rising plow bottom soil and is not impeded by any resistance from above, whereas the plow bottom layer experiences less disturbance.

As θ increases, the soil disturbance becomes more pronounced at the same depth. The main reason for this is that the shear and compression of the soil by the shovel tip intensify with increasing θ. More soil is sheared simultaneously, resulting in a greater accumulation of soil above the shovel tip, leading to a greater upward movement of the plow bottom layer. Hence, the soil disturbance becomes more evident.

Under the same θ, as the depth increases, the degree of soil disturbance gradually decreases. The main reason for this is that as the depth increases, although the shear and compression levels of the shovel tip increase, the presence of voids between the soil particles allows the rising soil to gradually fill these voids, resulting in a decreasing degree of soil disturbance.

By comparing the disturbance states of the plow bottom layer and the cultivation layer, the disturbance effects can be ranked as follows: chisel-shaped shovel > $\theta=0°$ shovel > $\theta=5°$ shovel > $\theta=1°$ shovel > $\theta=3°$ shovel.

Soil fragmentation effect

Existing studies have shown that excessive fragmentation of soil by subsoilers can increase the evaporation of soil moisture and hinder soil water retention(Qin *et al*., 2022). In order to assess the soil fragmentation effect during tillage, the quantity of broken bonds in the soil is used as an indicator. The variation of bond breakage quantity during the tillage process at different depths for subsoilers with different θ values is shown in Figure 7.

At 11.45s, the subsoiler has completely passed through the soil model. From Figure 7, it can be observed that as the depth increases, the number of bond breakages for each θ of the shovel increases. This is mainly because as the depth increases, the disturbed and sheared soil also

increases, leading to more soil fragmentation. At the same depth, the number of bond breakages for different θ values of the shovel remains consistent and is higher than that of the chisel-shaped shovel. This is primarily because the area of disturbed soil remains relatively consistent after tillage at the same depth, and the V-shaped structures and their quantities are consistent. At the same depth, the number of bond breakages in the shovel tips with different θ values remains consistent and is higher than that of the chisel-shaped shovel tip. This is primarily because, at the same depth, the disturbed soil area remains consistent for all shovel tips with V-shaped structures and the same quantity of V-shaped structures. On the other hand, the chisel-shaped shovel tip has fewer bond breakages due to the absence of a V-shaped structure. However, the difference in the number of bond breakages between the chisel-shaped shovel tip and the V-shaped shovel tip does not exceed 10%. Therefore, the V-shaped shovel tip does not result in excessive fragmentation(Tong *et al*., 2020).

Average resistance of tillage

Average resistance experienced by the subsoiler during the tillage process is shown in Figure 8. In the same tillage depth, the average resistance follows the order: θ=3° shovel tip < θ=5° shovel tip < θ=1° shovel tip< θ=0° shovel tip< chisel-shaped shovel tip. This is mainly because, at the same depth and under the same θ condition, the shear effect of the V-shaped structure is superior to the planar shear. The V-shaped structure facilitates the drainage of soil to the sides and the grooves between them act as conduits, allowing the soil to move in the opposite direction of tillage, thereby reducing the soil's resistance. Therefore, the chisel-shaped shovel experiences the highest resistance due to the absence of the V-shaped structure. As the angle θ increases, the V-shaped structure forms a smaller angle with the vertical direction of the soil. Therefore, within the same timeframe, more soil undergoes shearing. Additionally, the rate at which soil accumulates above the shovel tip is slower compared to the rate at which soil is directed away by the groove, resulting in a decrease in resistance when θ is between 0° and 3°. However, As the θ continues to increase, the speed of soil movement along the grooves between the V-shaped structures becomes slower than the rate of soil accumulation above the shovel tip. This leads to excessive soil accumulation above the shovel tip. Therefore, when θ is between 3° and 5°, the resistance increases. With increasing depth, the resistance experienced by the subsoiler with different θ values also increases. This is primarily due

to the increased shear and compression of the subsoiler as the depth increases, requiring more traction force and resulting in increased resistance.

The shovel tip with an angle θ of 5° ranks third in terms of soil disturbance and second in terms of reduction in resistance. The various V-shaped shovel tips exhibit similar performance in soil fragmentation. Therefore, the shovel tip with an angle of 5° demonstrates good overall performance. It achieves a reduction rate of 15.8% to 17.8% in resistance.

Soil disturbance validation

After the experiment, the coordinate parameters were obtained by the dot method on the interface photos. The contour curves of the tillage soil disturbance were fitted, and the profiles of the pit and ridge forms after tillage are shown in Figure 9..

The experimental results, as shown in Table 3, indicate that there is relatively small error between the simulated tillage process and the soil trough test. This suggests that the simulation model accurately simulates the soil disturbance behavior during tillage, and the V-shaped shovel tip with θ = 5° performs comparably to the chisel-shaped shovel tip.

Soil fragmentation validation

By calculating the soil fragmentation rates of the chisel deep-loosening shovel tip and the V-shaped shovel tip, they are 57.34±1% and 64.56±1%, respectively, with a difference of not exceeding 10%. In the simulation, the Bonds' breakage counts for the chisel tip and V-shaped tip do not exceed 10%, indicating that the simulation model is reasonably accurate.

Tillage resistance validation

The average resistance increases with the depth of tillage, whether using a V-shaped shovel tip or a chisel-shaped shovel tip, as shown in Figure 10 in both simulation models and soil trough experiments. However, from Figure 10, it can be observed that there is a significant discrepancy between simulation and experimental data. The main reason for this lies in the presence of impurities other than soil in the soil trough, such as grains, gravel, plant roots, etc. These factors were not considered in the simulation, leading to differences between simulation and experimental data, especially as the depth of tillage increases, the increase in impurities such as gravel results in a

significant increase in resistance in the soil trench experiment. Despite the substantial differences, both simulation and soil trough experiments indicate a reduction in resistance. In the soil trough experiment, the drag reduction effect of the V-shaped shovel tip can reach a maximum of 12.79%, with a minimum of 4.29%.

Conclusions

(1) To address the issue of high resistance at the shovel tip, this study draws inspiration from the V-shaped morphology of shark skin, which exhibits excellent drag reduction properties. Laser cladding technology is employed to create a V-shaped wear-resistant coating at the front end of the shovel tip surface. Additionally, the rear end of the shovel tip surface is designed to mimic the V-shaped structure of shark skin, and two enlarged V-shaped structures are proportionally incorporated to achieve drag reduction in the shovel tip.

(2) Through discrete element simulation, the average tillage resistance for three different H values at $\theta = 0°$ was obtained. After comparing the results, the shovel tip with the smallest tillage resistance at H = 40% was selected. Subsequently, a comprehensive analysis was conducted for four different θ values, considering soil disturbance, fragmentation, and tillage resistance. Based on this analysis, the V-shaped shovel tip with a θ of 5° was chosen. Compared to the chisel-shaped shovel tip, it achieves a drag reduction rate of 15.8% to 17.8%.

(3) By comparing the results of the chisel-shaped shovel tip and the V-shaped shovel tip with H of 40% and θ of 5° in both soil trough experiment and simulation, we observe noticeable differences between simulation and experimentation. However, under conditions ensuring optimal soil disturbance and fragmentation effects, both methods achieve a reduction in resistance. In the soil trough experiment, the H=40%, θ=5° V-shaped shovel tip demonstrates a drag reduction rate of 4.3% to 12.7% compared to the chisel-shaped shovel tip.

References

Zheng K., D. McHugh A., Li H.W., Wang Q.J., Lu C.Y., Hu H.N., Liu W.Z., Zhang Z.Q, Liu P., He J. 2019. Design and experiment of anti-vibrating and anti-wrapping rotary components for subsoiler cum rotary tiller. Int. J. Agric. Biol. Eng. 12:47-55.

Torres J.L.R., Leal Júnior A.L.B., Barreto A.C., Carvalho F.J., de Assis R.L., Loss A., Lemes E.M.,

Da Silva Vieira D.M. 2022. Mechanical and Biological Soil Decompaction for No-Tillage Maize Production. Agronomy-Basel. 12:2310.

Martins M.B., Marques Filho A.C., Santana L.S., Guimarães Júnnyor W.D.S., Bortolheiro F.P.D.A., Vendruscolo E.P., Seron C.D.C., Costa E., Da Silva K.G.P. 2023. Productivity and Quality Sugarcane Broth at Different Soil Management. Agronomy-Basel. 13:170.

Niu J.P., Luo T.Y, Xie J.Q, Cai H.X., Zhou Z.K, Chen J., Zhang S. 2022. Simulation and experimental study on drag reduction and anti-adhesion of subsoiler with bionic surface. Int. J. Agric. Biol. Eng. 15:57-64.

Song W., Jiang X.H., Li L.K., Ren L.L., Tong J. 2022. Increasing the width of disturbance of plough pan with bionic inspired subsoilers. Soil Tillage Res. 220:105356.

Zhang L., Zhai Y.B., Chen J.N., Zhang Z.E., Huang S.Z. 2022. Optimization design and performance study of a subsoiler underlying the tea garden subsoiling mechanism based on bionics and EDEM. Soil Tillage Res. 220:105375.

Wu B.G., Zhang R.Z., Hou P.F., Tong J., Zhou D.Y., Yu H.Y., Zhang Q., Zhang J.S, Xin Y.L. 2021. Bionic Nonsmooth Drag Reduction Mathematical Model Construction and Subsoiling Verification. Appl. Bionics Biomech. 2021:1-13.

Jia H.L., Guo M.Z., Zhao J.L., Huang D.Y., Zhuang J., Qi J.T. 2019. Design and test of bionic wide-ridge soybean tilling-sowing machine. Int. J. Agric. Biol. Eng. 12:42-51.

Bai J.F., li B., Lv X.T., Chen J., Shi J.T. 2016. Study on Vibration Anti-drag of tje Badger Claws Bionic Subsoiler. J. Agric. Mech. Res. 38:224-227. [Article in Chinese].

Zhang Z.H., Gan S.H., Zuo G.B., Tong J. 2021. Bionic Design and Performance Experiment of Sandfish Head Inspired Subsoiler Tine. Trans. Chin. Soc. Agric. Mach. 52:33-42. [Article in Chinese].

Ma F.L., Zeng Z.Z., Gao Y.M., Liu E.Y., Xue Q.J. 2016. Research status and progress of bionic surface drag reduction. Chin. Surf. Eng. 29:7. [Article in Chinese].

Wu L.Y., Jiao Z.B., Song Y.Q., Liu C.H., Wang H., Yan Y.Y. 2018. Experimental investigations on drag-reduction characteristics of bionic surface with water-trapping microstructures of fish scales. Sci Rep. 8:12186–12191.

Pu X, Li G, Liu Y. 2016. Progress and perspective of studies on biomimetic shark skin drag reduction. Chem Bio Eng Reviews. 3:26–40.

ZHANG D.Y., LUO Y.H., LI X., CHEN H.W. 2011. NUMERICAL SIMULATION AND EXPERIMENTAL STUDY OF DRAG-REDUCING SURFACE OF A REAL SHARK SKIN. J. Hydrodyn. 23:204-211.

Wen L., Weaver J.C., Lauder G.V. 2014. Biomimetic shark skin: design, fabrication and hydrodynamic function. J. Exp. Biol. 217(10):1656-1666.

Sun J.Y., Wang Y.M., Ma Y.H., Tong J., Zhang Z.J. 2018. DEM simulation of bionic subsoilers (tillage depth >40 cm) with drag reduction and lower soil disturbance characteristics. Adv. Eng. Softw. 119:30-37.

Wang X.Z. 2021. Soil-Winged Subsoiler Interactions and Their Effects. Northwest A&F University.

Hu H.B., Song B.W., Pan G., Mao Z.Y., Du X.H. 2007. Simulation Studies On Drag Reduction Mechanism of Shark Riblets Surface. J. Syst. Simul. 4901-4903. [Article in Chinese].

Wang Y.M., Li N., Ma Y.H, Tong J., Pfleging W., Sun J. 2020. Field experiments evaluating a biomimetic shark-inspired (BioS) subsoiler for tillage resistance reduction. Soil Tillage Res. 196:104432.

Zhao D.Y., Huang Z.P., Wang M.J., Wang T., Jin Y.F. 2012. Vacuum casting replication of micro-riblets on shark skin for drag-reducing applications. J. Mater. Process. Technol. 212:198-202.

Kim T.W. 2014. Assessment of Hydro/Oleophobicity for Shark Skin Replica with Riblets. J. Nanosci. Nanotechnol. 14:7562-7568.

Dean B., Bhushan B. 2010. Shark-skin surfaces for fluid-drag reduction in turbulent flow: a review. Philos. Trans. R. Soc. A-Math. Phys. Eng. Sci. 368:4775-4806.

Yan Z.F., Li M.D., Du Z.H., Yang X., Luo Y., Chen X.D., Han B. 2023. Study on a tracked amphibious robot bionic fairing for drag reduction. Ocean Eng. 267.

Agrawal A.K., Chattopadhyaya S., Murthy V.M.S.R., Legutko S., Krolczyk G. 2020. A Novel Method of Laser Coating Process on Worn-Out Cutter Rings of Tunnel Boring Machine for Eco-Friendly Reuse. Symmetry-Basel. 12:471.

Xu L.F, Song Z.H., Li M.X., Li F., Guo J., Gao M. 2021. Self-Grinding Silage Knife Strengthened with Ni–WC Alloy Prepared by Laser Cladding. Appl. Sci.-Basel. 11:10236.

Shan B., Chen J.L., Chen S.Y., Ma M.Z., Ni L.L., Shang F.M., Zhou L. 2022. Laser cladding of Fe-based corrosion and wear-resistant alloy: Genetic design, microstructure, and properties.

Surf. Coat. Technol. 433:128117.

Li M.K., Huang K.P., Yi X.M. 2023. Crack Formation Mechanisms and Control Methods of Laser Cladding Coatings: A Review. Coatings 13:1117.

Chen H.W., Che D., Zhang X., Yue Y., Zhang D.Y. 2015. Large-proportional shrunken bio-replication of shark skin based on UV-curing shrinkage. J. Micromech. Microeng. 25.

Wang W.W., Song J.L., Zhou G.A., Quan L.Z., Zhang C.L., Chen L.Q. 2022. Development and Numerical Simulation of a Precision Strip-Hole Layered Fertilization Subsoiler While Sowing Maize. Agriculture-Basel. 12:938.

Li X., Jiang Z.J., Wang S.C., Li X.L., Liu Y., Wang X.H. 2023. A Study of a Model   for Predicting Pneumatic Subsoiling Resistance Based on Machine Learning Techniques. Agronomy-Basel. 13:1079.

Zheng K., He J., Li H.W., Diao P.S., Wang Q.J., Zhao H.B. 2016. Research on Polyline Soil-breaking Blade Subsoiler Based on Subsoiling Soil Model Using Discrete Element Method. Trans. Chin. Soc. Agric. Mach. 47:9. [Article in Chinese].

Ding Q.S., Ren J., BELAL E.A., Zhao J.K., Ge S.Y., Li Y. 2017. DEM Analysis of Subsoiling Process in Wet Clayey Paddy Soil. Trans. Chin. Soc. Agric. Mach. 48:3. [Article in Chinese].

Wang Y., Zhang D., Yang L., Cui T., Jing H., Zhong X. 2020. Modeling the interaction of soil and a vibrating subsoiler using the discrete element method. Comput. Electron. Agric. 174:105518.

Hao Z.H., Zheng E.L., Li X., Yao H.P., Wang X.C., Qian S.Y., Li W.X., Zhu M. 2023. Performance analysis of the soil-contacting parts for no-tillage planters and optimization of blade structure. Trans. Chin. Soc. Agric. Eng. 39:2. [Article in Chinese].

Jiang X.H., Tong J., Ma Y.H., Sun J.Y. 2020. Development and verification of a mathematical model for the specific resistance of a curved subsoiler. Biosyst. Eng. 190:107-119.

Wang X.Z., Li P., He J.P., Wei, W., Huang Y.X. 2021. Discrete element simulations and experiments of soil-winged subsoiler interaction. Int. J. Agric. Biol. Eng. 14:50-62.

Wang X.Z., Zhang S., Pan H.B., Zheng Z.Q., Huang Y.X., Zhu R.X. 2019. Effect of soil particle size on soil-subsoiler interactions using the discrete element method simulations. Biosyst. Eng. 182:138-150.

Vanderhasselt A., Cool S., D Hose T., Cornelis W. 2023. How tine characteristics of subsoilers affect fuel consumption, penetration resistance and potato yield of a sandy loam soil. Soil

Tillage Res. 228:105631.

Qin K., Zhao Y., Zhang Y.Z., Cao C.M., Shen Z.G. 2022. Lateral stress and its transmission law caused by operation of a double-wing subsoiler in sandy loam soil. Front. Environ. Sci. 10.

Tong J., Jiang X.H., Wang Y.M., Ma Y.H., Li J.W., Sun J.Y. 2020. Tillage force and disturbance characteristics of different geometric-shaped subsoilers via DEM. Adv. Manuf. 8:392-404.

(a) Schematic diagram of subsoiler

(b) Chisel-shaped shovel tip

(c) Microscopic structure of shark skin

(d) V-shaped shovel tip

$$H = \frac{S_{Brown}}{S_{Semicircle}}$$
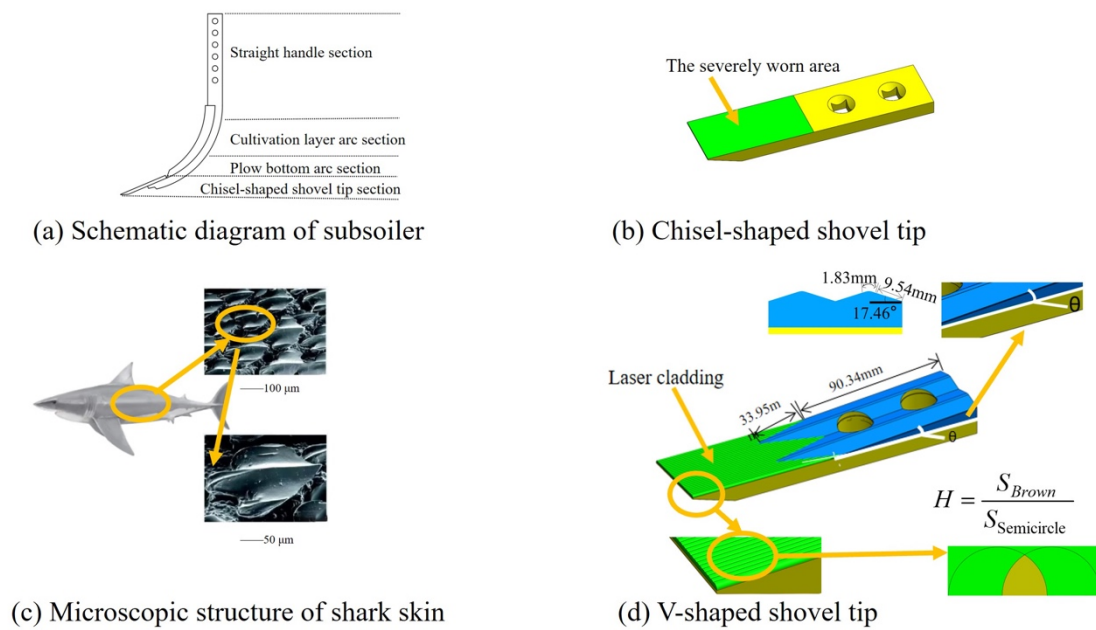
Figure 1. The process of Shovel tip design.

(a) Schematic diagram of diversion

(b) The diagram of soil particle

(c) The diagram of soil disturbance
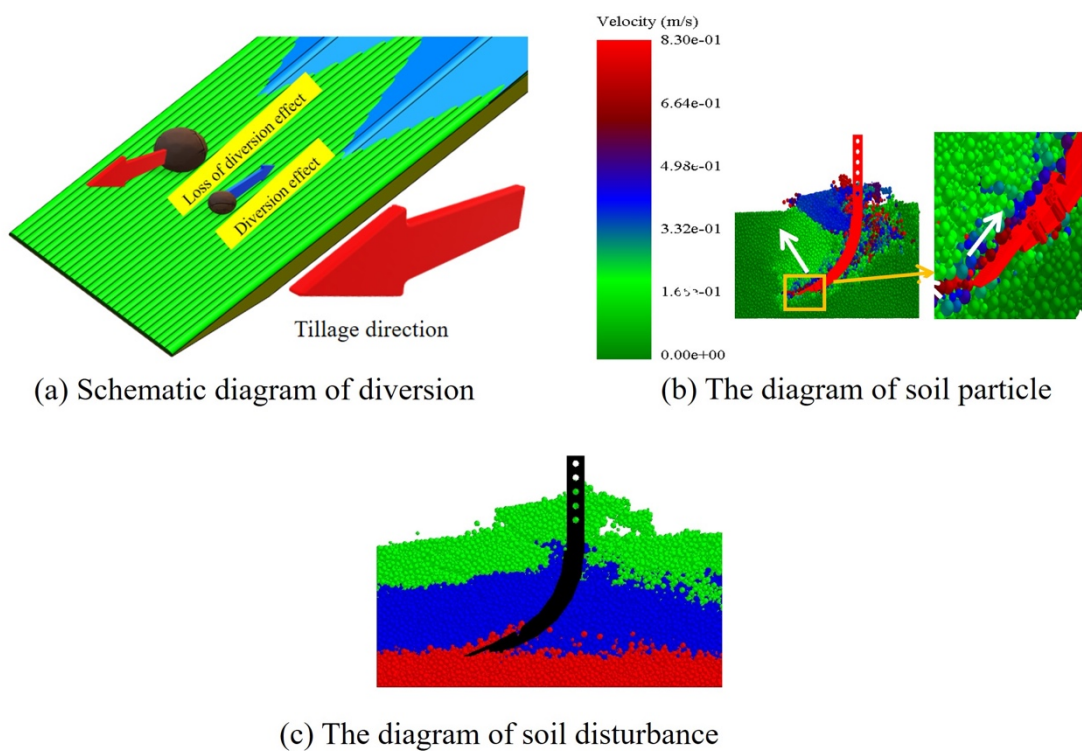
Figure 2. The working diagram of V-shaped Shovel Tip.

(a) The model of subsoiler

(b) Simulation model of EDEM

(c) Cylindrical bonds between soil particles
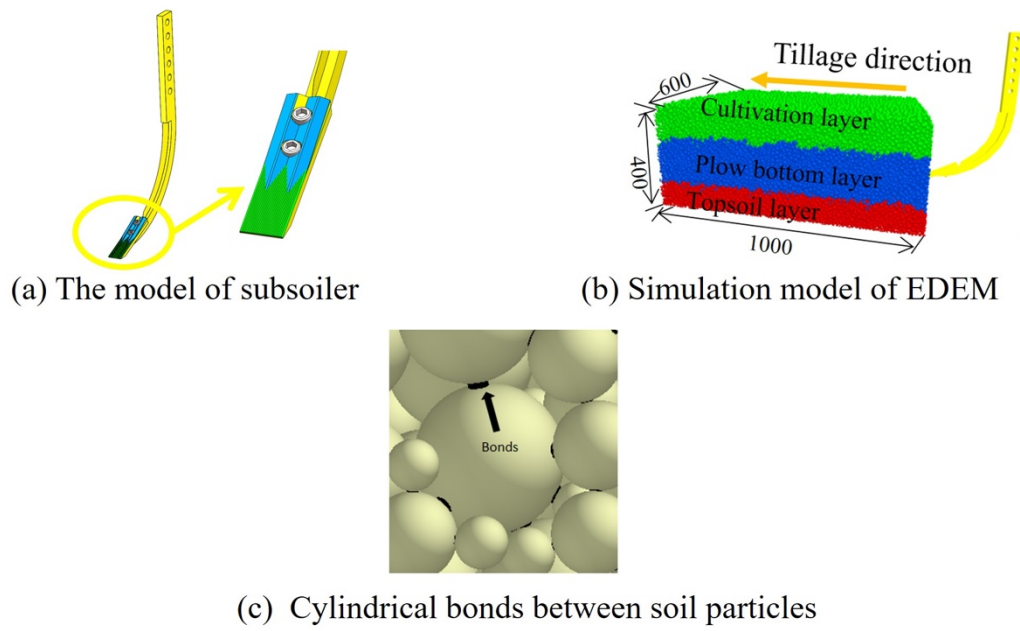
Figure 3. The model of simulation.

(a) Moisture content adjustment

(b) Moisture content measurement

(c) Compaction testing

(d) Tillage area

(e) Shovel tip

(f) Rotary tillage operation

(g) Compaction operation

(h) Subsoiling operation
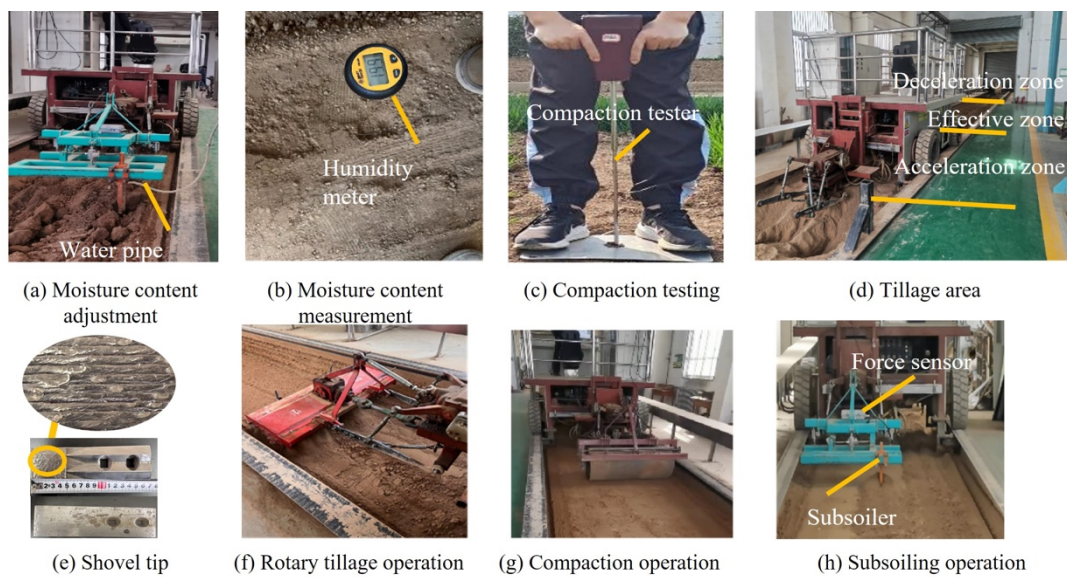
Figure 4. Tillage experiment process.
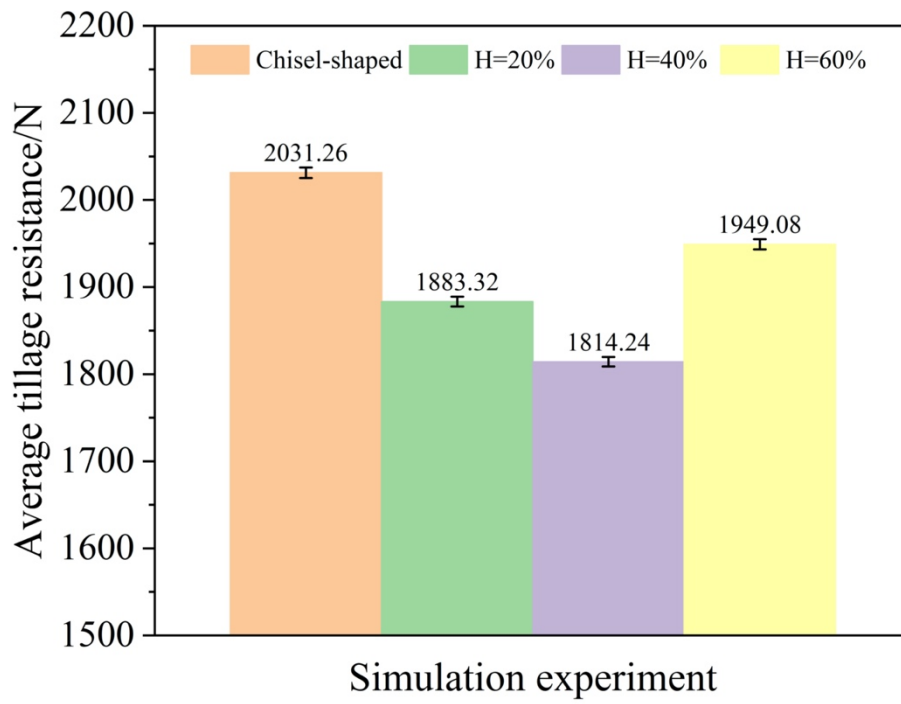
Figure 5. The impact of H on tillage resistance.
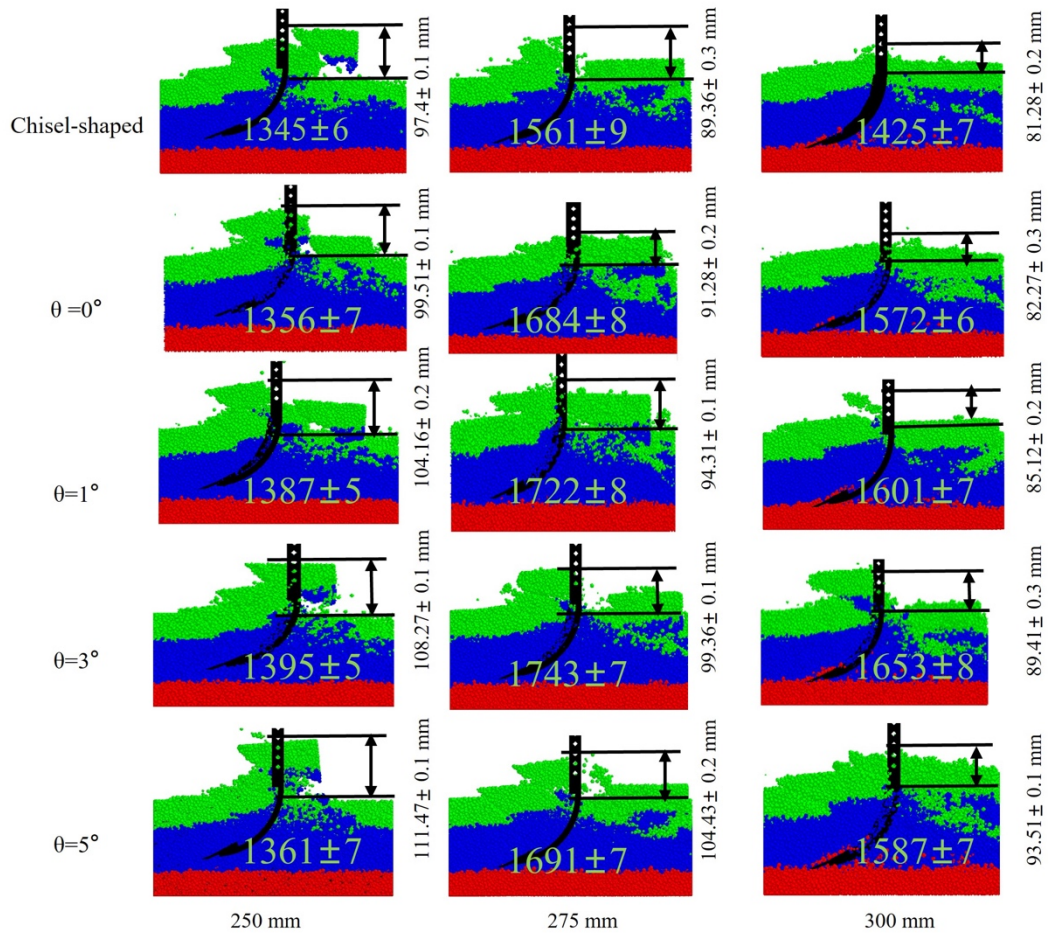
Figure 6. Disturbance effect of different back-dip angles on soil.
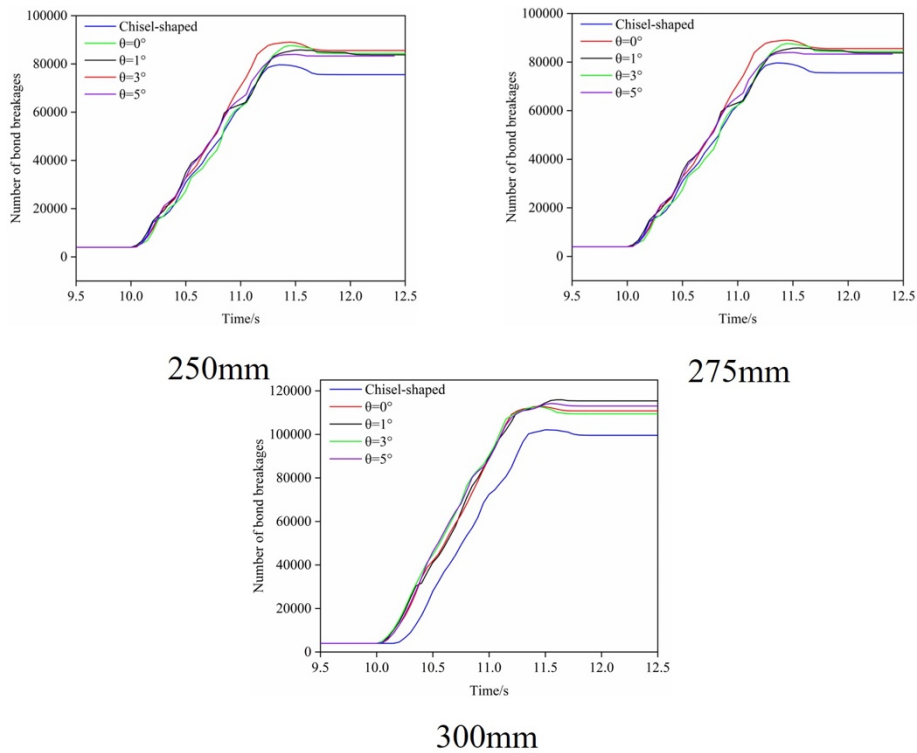
Figure 7. The number of bond breakages at different subsoiling depths.
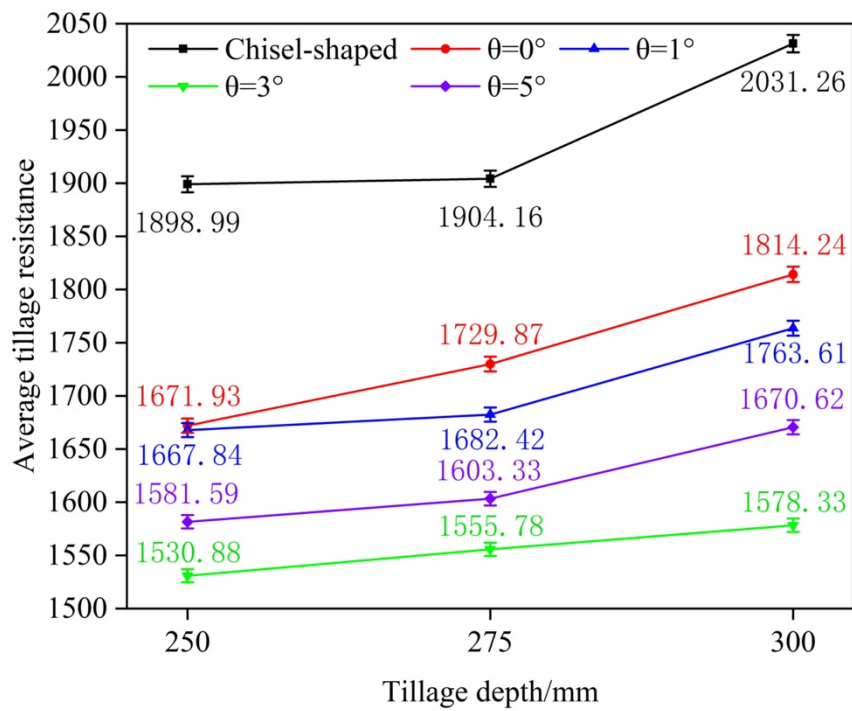
Figure 8. The impact of θ on tillage resistance.
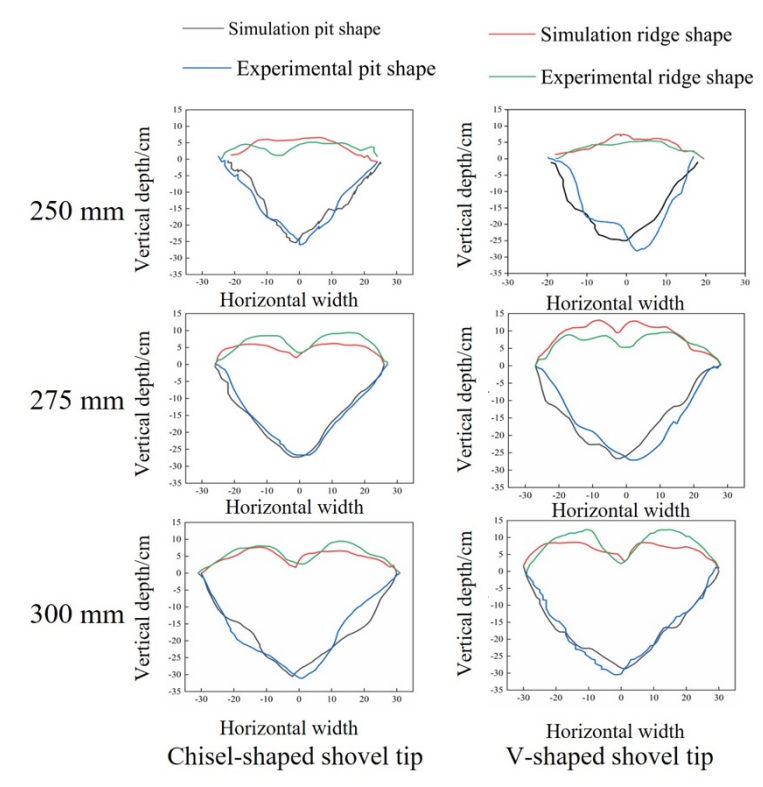
Figure 9. Soil trough cross section diagram.
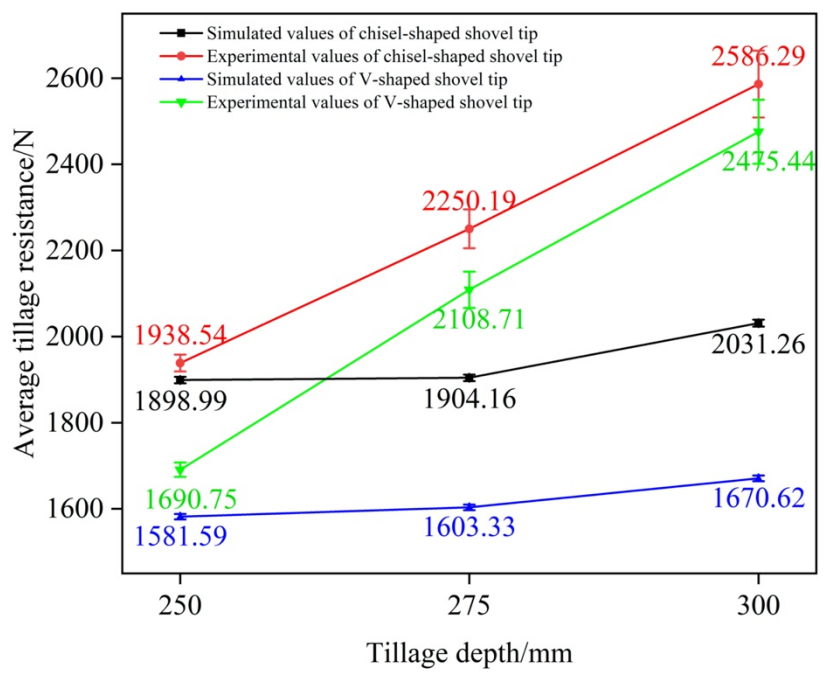
Figure 10. Comparison of resistance in simulation with resistance from soil trough experiment.

Table 1. Particle size and distribution in various soil layers.

Soil layering / Particle size d/mm	d＞6	6≥d≥4	d＜4
Cultivation layer	52.25%	15.09%	32.66%
Plow bottom layer	58.16%	28.33%	13.51%
Topsoil layer	58.17%	16.12%	25.71%

Table 2. Basic parameters of the EDEM model.

Parameter	Value		
The depth of soil/mm	0-220	220-300	300-400
Soil particle size of 8mm/%	52	58	58
Parameter	Value		
Soil particle size of 5mm/%	15	28	16
Soil particle size of 3mm/%	33	14	26
Poisson's ratio of top soil	0.4	0.42	0.41
Density of the soil/（kg/m^3）	1360	1730	1610
Shear modulus of top soil/Pa	6×10^7	1×10^8	1×10^8
Coefficient of static friction between soil	0.375	0.389	0.388
Coefficient of rolling friction between soil	0.56	0.24	0.23
Soil moisture content	17.79%	21.19%	21.92%
Poisson's ratio of 65Mn steel	0.3		
Density of 65Mn steel/（kg/m^3）	7850		
Shear modulus of 65Mn steel/Pa	7.85×10^{10}		
Coefficient of rolling friction between soil and 65Mn steel	0.34	0.14	0.26
Coefficient of static friction between soil and 65Mn steel	0.647	0.584	0.754

Table 3. Cross-sectional area of soil trough.

Types of shovel tips	Depth/mm	Simulated values/mm³	Experimental values/mm³	Error/%
Chisel-shaped shovel tip	250	768.95	802.81	4.22
	275	1071.21	1204.47	11.06
	300	1370.15	1400.06	2.14
V-shaped shovel tip	250	659.52	698.09	5.52
	275	1214.9	1317.17	7.76
	300	1437.08	1518.83	5.38